Dalton Transactions

ROYAL SOCIETY OF CHEMISTRY

COMMUNICATION

View Article Online
View Journal | View Issue

Cite this: *Dalton Trans.*, 2026, **55**, 1646

Received 24th November 2025,
Accepted 3rd January 2026

DOI: 10.1039/d5dt02801a

rsc.li/dalton

A one-dimensional selenotungstate based on neodymium and {SeO_3} groups for catalytic synthesis of imidazoles

Hao-Zhe Wang,[a] Yu-Feng Liu,*[a] Zhou-Fu Lin,[a] Shi-Xiong Li *[b] and Guo-Ping Yang *[a]

A novel neodymium-{SeO_3}-bridged selenotungstate, [$Na_{16}Nd_{2.5}(SeO_3)(SeO_3)(mal)(W_4O_9)(SeW_8O_{32})(SeW_9O_{33})_2(H_2O)_4$]·*ca.*$26H_2O$ (NdSeW, mal = malic acid), has been successfully synthesized and structurally characterized. This compound is constructed from both {SeW_9} and {SeW_8} building units, which are linked through an organometallic {$Nd_2Se_2(mal)W_4$} cluster, forming a distinctive triangular arrangement. Two triangular trimers are connected *via* Nd–O–W to form a hexameric unit, which is subsequently extended into a one-dimensional chain structure through bridging by two {SeO_3} groups. This type of one-dimensional chain architecture, constructed through alternating connections involving neodymium and {SeO_3} groups, is extremely rare in polyoxometalate chemistry. In addition, NdSeW exhibits excellent catalytic activity for the synthesis of 2,4,5-trisubstituted imidazoles through the three-component condensation of aldehydes, benzils, and ammonium acetate under environmentally benign conditions.

Introduction

Polyoxometalates (POMs) represent a class of nanoscale metal–oxygen clusters with diverse structural architectures and functional properties, garnering significant interest in the fields of materials science and catalysis.[1–9] These clusters are predominantly composed of early transition metals such as tungsten, molybdenum, and vanadium in high oxidation states and exhibit remarkable versatility due to their tunable acidity, redox behavior, and ability to incorporate various heteroatoms and metal cations.[10–14] Among these, lanthanide-containing POMs (Ln-POMs) have emerged as promising materials owing to the unique coordination flexibility and Lewis acidity of lanthanide ions, which facilitate the construction of novel structures and enhance catalytic performance.[6,15–17]

The incorporation of selenium as a heteroatom in POM chemistry has enabled significant advances in structural diversification. Selenium functions not only as a templating agent but also as a bridging unit, facilitating the construction of novel architectures that are uncommon in conventional POM systems.[18–21] Notably, lanthanide-functionalized selenotungstates provide a versatile platform for designing multifunctional materials with promising applications in catalysis, sensing, and molecular magnetism.[22–24]

Despite significant advancements, the integration of multiple building blocks within a single POM framework remains challenging due to variations in stability and reactivity among precursor fragments.[25–27] Utilizing lanthanide ions as structural linkers provides a viable strategy to mitigate these limitations, enabling the assembly of complex structures incorporating heterogeneous building units.[13,20] In this context, neodymium, characterized by its high coordination number and pronounced Lewis acidity, represents an interesting candidate for constructing novel POMs.

Herein, we report the synthesis and structural characterization of a novel neodymium–{SeO_3}-bridged selenotungstate, [$Na_{16}Nd_{2.5}(SeO_3)(SeO_3)(mal)(W_4O_9)(SeW_8O_{32})(SeW_9O_{33})_2(H_2O)_4$]·*ca.*$26H_2O$ (**NdSeW**), which incorporates both {SeW_9} and {SeW_8} building units stabilized by an organometallic {$Nd_2Se_2(mal)W_4$} cluster. This compound features a unique triangular arrangement and further self-assembles into a one-dimensional chain through Nd–O–W and {SeO_3} linkages. Moreover, **NdSeW** exhibits excellent catalytic performance in the synthesis of 2,4,5-trisubstituted imidazoles through the three-component condensation of aldehydes, benzils, and ammonium acetate. This work not only expands the structural diversity of Ln-containing selenotungstates but also highlights their potential as efficient catalysts under mild and environmentally benign conditions.

Results and discussion

Crystal structural description of NdSeW

NdSeW crystallizes in the monoclinic space group *C*2/*c* (Table S1) and its molecular skeleton comprises a trimeric

[a]*Jiangxi Province Key Laboratory of Functional Organic Polymers, Jiangxi Key Laboratory for Mass Spectrometry and Instrumentation, East China University of Technology, Nanchang 330013, China. E-mail: erick@ecut.edu.cn, yfliu@ecut.edu.cn*
[b]*School of Mechanical and Resource Engineering, Wuzhou University, Wuzhou, Guangxi 543003, P. R. China. E-mail: lsx1324@163.com*

polyoxoanion $[Nd_{2.5}(SeO_3)(SeO_3)(mal)(W_4O_9)(SeW_8O_{32})(SeW_9O_{33})_2(H_2O)_4]^{16-}$. Bond-valence-sum (BVS) analysis indicated that all Nd and W atoms exhibit oxidation states of +3 and +6, respectively (Table S2). As exhibited in Fig. 1a, the structure of compound **NdSeW** features one $\{Nd_{0.5}SeW_8\}$ building unit capping a dimeric $\{Nd_2Se_2(mal)W_4(SeW_9)_2\}$ fragment (Fig. 1a and b). This configuration arises through substitution of a tungsten position in the $\{SeW_9\}$ unit by an Nd3 atom, generating the $\{Nd_{0.5}SeW_8\}$ cluster (Fig. 1h). Concurrently, the organometallic linker cluster $\{Nd_2Se_2(mal)W_4\}$ bridges two $\{SeW_9\}$ units, thus constituting the $\{Nd_2Se_2(mal)W_4(SeW_9)_2\}$ framework (Fig. 1b–d). **NdSeW** also displays a triangular arrangement of two trivacant Keggin $\{SeW_9\}$ anionic units and one $\{SeW_8\}$ anionic unit connected by an $\{Nd_{2.5}Se_2W_4(mal)\}$ cluster, thereby forming a distinct triangular configuration (Fig. 1e). This linker stabilizes the trimeric assembly through the formation of W–O–W, W–O–Nd, and W–O–Se bonds between the cluster and the $\{SeW_9\}$ or $\{SeW_8\}$ polyoxoanions (Fig. 1a and e–g). Within the $\{Nd_{2.5}Se_2W_4(mal)\}$ cluster, the oxygen atoms (O82 and O83) of the DL-malic acid ligand coordinate to W21, generating a five-membered chelate ring (Fig. 1i). The three Nd centers (Nd1, Nd2, and Nd3) connect to peripheral tungsten and selenium atoms *via* metal–oxygen–metal (M–O–M) linkages. All three Nd^{3+} ions adopt a distorted octacoordinate geometry (Fig. S1). Nd1 is coordinated through oxygen-sharing to six μ_2-O atoms from $\{WO_6\}$ octahedra (W9, W19, W22, W26, W28, and W30), one μ_2-O atom from a $\{SeO_3\}$ unit (Se5), one μ_2-O atom from a sodium center (Na1), and one μ-O atom from a water molecule (Fig. 1j). Nd2 is coordinated through oxygen-sharing to five μ_2-O atoms from $\{WO_6\}$ octahedra (W9, W12, W13, W19, and W30), one μ_2-O atom from a $\{SeO_3\}$ unit (Se4), one μ_2-O atom from a sodium center (Na4), and one μ-O atom from a water molecule (Fig. 1k). Notably, the Nd3 site exhibits positional disorder over two symmetry-equivalent positions (occupancy 0.5 each), with each Nd^{3+} ion coordinated *via* four μ_3-O bridges linking to Na2, Se5, and W6, and four μ_2-O bridges connecting to W2 and W5 (Fig. 1l). The bond distances of Nd–O range from 2.330 to 2.566 Å (Table S2).

Dimerization occurs between two adjacent trimeric clusters *via* key structural linkers comprising two Na^+ ions (Na5), the fractionally occupied Nd3 site, and two DL-malic acid ligands (Fig. S2). This distinctive dimer adopts a distorted configuration characterized by an ideal dihedral angle of precisely 78.783° between the planes defined by the constituent trimeric clusters (Fig. 2a and c). The Nd3 center bridges the dimeric units through coordination to four μ_2-O atoms originating from W6 and W28. Each DL-malic acid ligand exhibits dual-bridging functionality: one carboxylate terminus coordinates Na5, which is simultaneously bound to the μ_2-O donor from W6, while the opposing carboxylate group chelates W28 *via* two μ_2-O atoms. Sodium atoms occupy peripheral positions

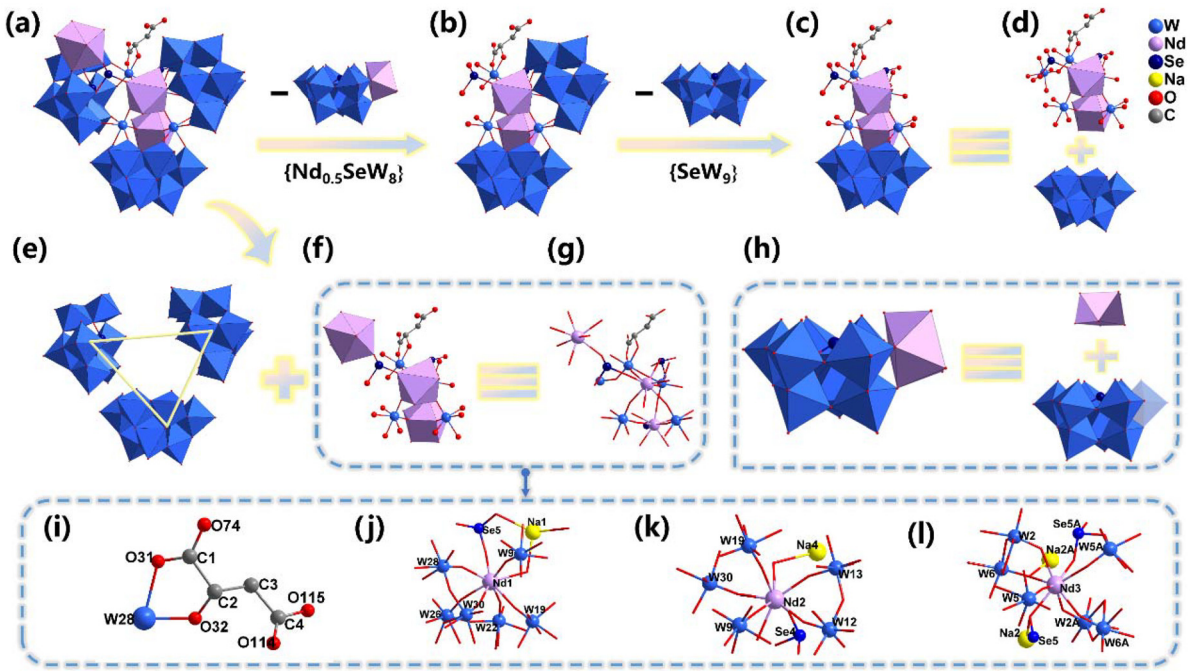

Fig. 1 (a) The structure of **NdSeW**. (b) The $\{Nd_2Se_2(mal)W_4(SeW_9)_2\}$ fragment formed by removing the $\{Nd_{0.5}SeW_8\}$ cluster from **NdSeW**. (c) The $\{Nd_2Se_2(mal)W_4SeW_9\}$ fragment formed by removing one $\{SeW_9\}$ cluster from the $\{Nd_2Se_2(mal)W_4(SeW_9)_2\}$ fragment. (d) The $\{Nd_2Se_2(mal)W_4SeW_9\}$ fragment is composed of a $\{SeW_9\}$ cluster unit and an organometallic $\{Nd_2Se_2(mal)W_4\}$ cluster unit. (e) The arrangement of two $\{SeW_9\}$ and one $\{SeW_8\}$ units showing the triangular motif. (f) and (g) The $\{Nd_{2.5}Se_2(mal)W_4\}$ cluster. (h) The substitution of a $\{WO_6\}$ octahedral unit within the trivacant Keggin-type $\{SeW_9\}$ cluster by a $\{NdO_8\}$ moiety. (i) Coordination mode of the DL-malic acid ligand. (j), (k) and (l) Coordination modes of Nd1, Nd2, and Nd3, respectively.

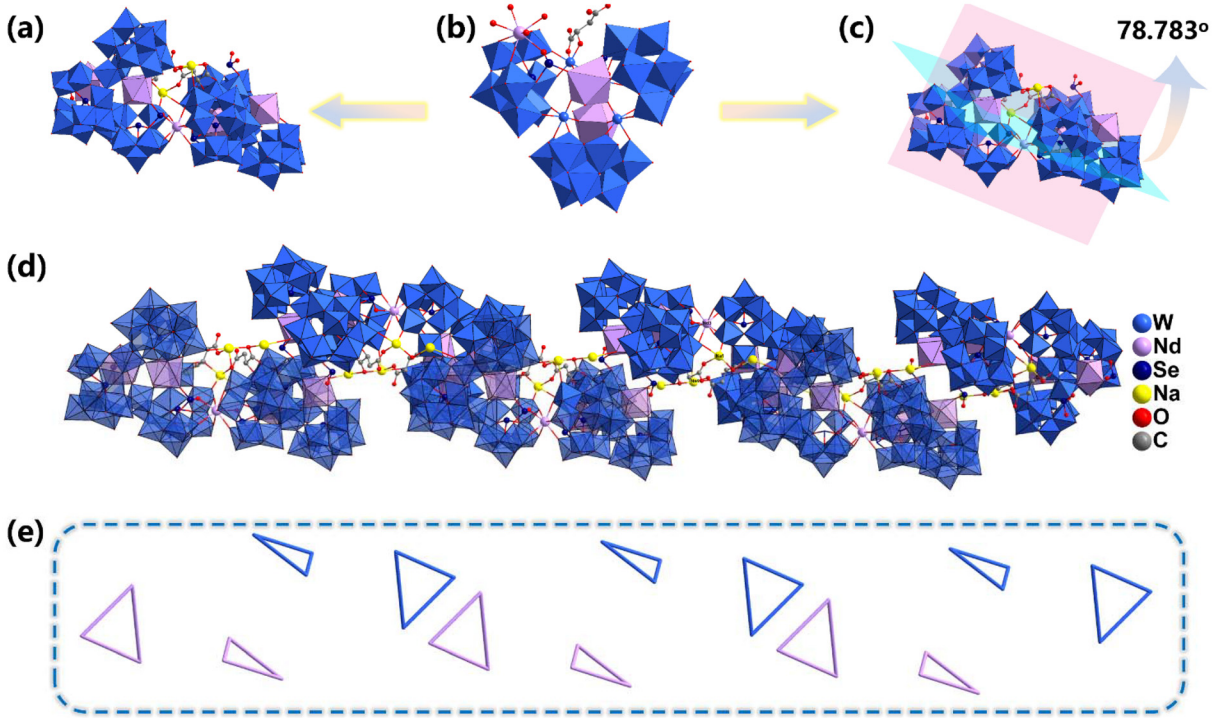

Fig. 2 (a) The dimer of compound **NdSeW** formed through bridging by Nd and Na atoms. (b) The structure of **NdSeW**. (c) The angle between the two monomeric units constituting the dimer of compound **NdSeW**. (d) The one-dimensional chain of **NdSeW**. (e) Schematic representation of the 1D chain of **NdSeW**, using triangles to represent monomeric units.

around the dimeric units of **NdSeW**, playing critical roles in stabilizing the nanocluster assembly. This structural motif extends into a 1D chain (Fig. 2d) through alternating the vertical connectivity of dimeric clusters, where adjacent triangular clusters maintain parallel orientation (Fig. S3). Within this architecture, two Se4 atoms bridge neighboring clusters *via* coordination to two Nd2 atoms (through O atoms) and two W30 atoms from triangular subunits. Simultaneously, two Na4 atoms consolidate the chain by dual-bridging interactions: they coordinate two Nd2 atoms while linking two DL-malic acid ligands through oxygen bridges, thereby providing essential stabilization to the 1D framework (Fig. S4). In Fig. 2e, the 1D chain architecture is visualized with displaced 1a dimeric units represented as pink triangles and conventional **NdSeW** units as blue triangles. This color-coded scheme distinctly reveals the alternating vertical stacking pattern of dimeric clusters, where all triangular units maintain strict parallel alignment along the chain axis.

Furthermore, Fourier transform infrared (FT-IR) spectroscopy and X-ray diffraction (XRD) were employed to further verify the structure of **NdSeW**. XRD measurements (Fig. S5) confirmed the phase purity of **NdSeW**, as evidenced by the consistency between the experimental diffraction peaks and those in the simulated pattern. Meanwhile, the FT-IR analysis (Fig. S6) revealed vibrational modes commensurate with a lacunary Keggin-type architecture. The spectrum showed ν(W–O–W) bridges at 780 and 832 cm^{-1}, terminal ν(W=O) bonds at 957 cm^{-1}, and ν(Se–O) vibrations at 1052 cm^{-1}. Features associated with the DL-malic acid ligand were also discernible, with C=O and C–O stretching vibrations occurring at 1621 and 1416 cm^{-1}, respectively, validating its coordination. Finally, a broad band centered at 3407 cm^{-1} was indicative of O–H stretches from water molecules.

Catalytic performance

Imidazole, a significant heterocyclic compound, is extensively utilized in various fields including biomedicine, materials science, and organic synthesis.[28–30] The conventional synthesis of imidazole derivatives typically involves the acid-catalyzed condensation reaction of aldehydes, benzils, and ammonium acetate.[31–35] However, existing catalytic systems are associated with several limitations, such as environmental contamination caused by metal catalysts and organic solvents, long reaction times, harsh reaction conditions, and complicated operational procedures.[36,37] Therefore, the development of an efficient, practical, and environmentally friendly catalytic system remains highly desirable and urgently needed. Considering the unique Lewis acid catalytic activity of rare-earth (RE) elements and our experience in RE-POM catalysis, the application of **NdSeW** as a catalyst for the condensation reaction of aldehydes, benzils, and ammonium acetate presents a promising approach for the synthesis of imidazoles.

Therefore, we selected the three-component condensation reaction of benzaldehyde (**1a**, 0.2 mmol), benzil (**2a**,

0.2 mmol), and ammonium acetate (**3a**, 0.6 mmol) to evaluate the catalytic performance of **NdSeW** (Table 1). Under solvent-free conditions at 80 °C for 2 h, the yields of the desired product **4a** with and without **NdSeW** were 57% and 10%, respectively (Table 1, entries 1 and 2). These results indicate that **NdSeW** indeed exhibits significant catalytic activity for this reaction. Subsequently, the influence of a series of green solvents, including dimethyl carbonate (DMC), ethyl acetate (EA), water, and EtOH, on the reaction yield was investigated. The addition of DMC, EA, and water did not have a positive effect; however, when EtOH was used as the solvent, the yield increased to 72% (Table 1, entries 3–6). When the reaction temperature was raised to 90 °C, the yield increased to 85%, and further increasing the temperature did not result in a significant improvement in yield. When the reaction was carried out for 3 h, the yield of **4a** reached 97%. When the catalyst loading was reduced to 0.4 mol%, the yield significantly decreased to 88%. Further increasing the catalyst loading did not lead to a better result. Thus, the optimal catalytic conditions were determined as follows: benzaldehyde (**1a**, 0.2 mmol), benzil (**2a**, 0.2 mmol), ammonium acetate (**3a**, 0.6 mmol), **NdSeW** (0.5 mol%), and ethanol (1 mL), reacted at 90 °C for 3 h. Furthermore, we summarized and compared this catalytic system with those previously reported for constructing imidazole compounds (Table S3). The results demonstrate that **NdSeW** offers advantages in this reaction, including a low catalyst loading and high product yield.

Subsequently, to evaluate the compatibility of this catalytic system, various aldehydes and benzils were used to prepare 2,4,5-trisubstituted imidazole derivatives (Table 2). First, the reactivity of a series of aldehydes containing electron-donating and electron-withdrawing groups was investigated.

Table 1 Optimization of reaction conditions[a]

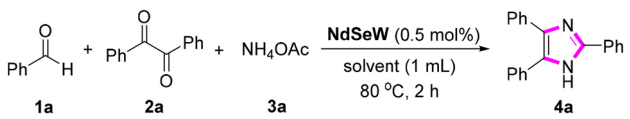

Entry	Solvent	Temperature (°C)	Time (h)	Yield[b] (%)
1[c]	Solvent-free	80	2	10
2	Solvent-free	80	2	57
3	DMC	80	2	32
4	EA	80	2	41
5	H_2O	80	2	9
6	EtOH	80	2	72
7	EtOH	90	2	85
8	EtOH	100	2	86
9	EtOH	90	2.5	92
10	EtOH	90	3	97
11[d]	EtOH	90	3	88
12[e]	EtOH	90	3	96

[a] Reaction conditions: benzaldehyde (**1a**, 0.2 mmol), benzil (**2a**, 0.2 mmol), ammonium acetate (**3a**, 0.6 mmol), solvent (1 mL), and **NdSeW** (0.5 mol%) for 2 h. [b] The yields were determined by GC with biphenyl as the internal standard. [c] Without a catalyst. [d] Catalyst loading: 0.4 mol%. [e] Catalyst loading: 0.6 mol%.

Table 2 NdSeW-catalyzed synthesis of imidazoles[a,b]

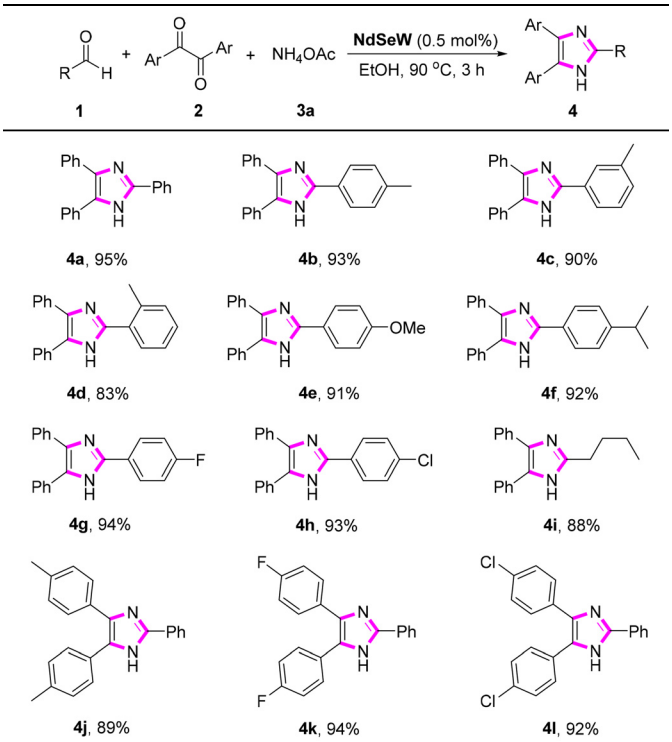

[a] Reaction conditions: benzaldehyde (**1a**, 0.2 mmol), benzil (**2a**, 0.2 mmol), ammonium acetate (**3a**, 0.6 mmol), EtOH (1 mL), **NdSeW** (0.5 mol%), and 90 °C for 3 h. [b] Isolated yield.

Benzaldehydes with electron-donating groups (such as –Me, –OMe, and –^{i}Pr) reacted smoothly with benzaldehyde and ammonium acetate, affording the corresponding imidazole products in 83%–93% yields (**4a–4f**). The steric hindrance of the benzaldehyde had a certain influence on the yield, as evidenced by the gradually decreasing yields observed for *p*-, *m*-, and *o*-methyl-substituted benzaldehydes. Benzaldehydes containing electron-withdrawing groups (such as –F and –Cl) were also effectively converted into the corresponding desired products, with yields of 94% and 93%, respectively (**4g–4h**). Furthermore, aliphatic aldehyde was well tolerated under this catalytic system; for instance, *n*-pentanal was converted into the desired product **4i** in 88% yield. A series of 4,4′-disubstituted benzil compounds, such as 4,4′-dimethylbenzil, 4,4′-dichlorobenzil and 4,4′-dibromobenzil, also reacted efficiently with benzaldehyde and ammonium acetate, affording the corresponding products in 89%–94% yields (**4j–4l**).

Finally, we investigated the stability and recyclability of **NdSeW**. PXRD analysis of the catalyst before and after the reaction revealed no significant differences between the recovered and as-synthesized **NdSeW** (Fig. S5). Furthermore, catalytic cycling experiments were conducted to evaluate the reusability of **NdSeW**. There was no notable decrease in product yield after five consecutive cycles (Fig. 3a). This preliminary result indicates that **NdSeW** exhibits basic stability and recoverability under the tested conditions. To identify the active sites of

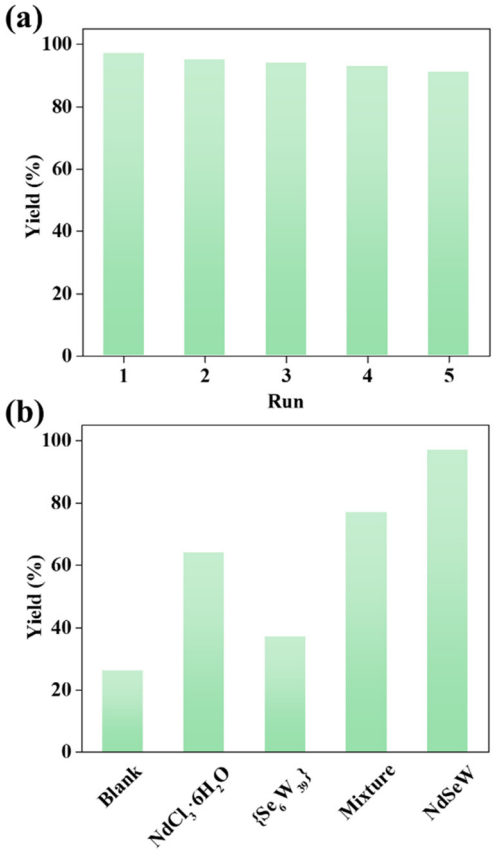

Fig. 3 (a) The cycling experiments and (b) the control experiments.

NdSeW and explore the reaction mechanism, a series of control experiments was performed. As shown in Fig. 3b, both $NdCl_3{\cdot}6H_2O$ and $(NH_4)_6Na_{18}[Se_6W_{39}O_{141}(H_2O)_3]{\cdot}60H_2O$ ($\{Se_6W_{39}\}$) were able to promote the reaction, but the yield obtained with $NdCl_3{\cdot}6H_2O$ was higher than that with $\{Se_6W_{39}\}$, suggesting that Nd^{3+} plays a dominant role in the catalysis. Notably, the catalytic efficiencies of $NdCl_3{\cdot}6H_2O$, $\{Se_6W_{39}\}$, and their mixture were all lower than that of **NdSeW**, indicating that the well-defined crystalline structure has a positive effect on the catalytic activity. Based on relevant reports and the above results,[38,39] a plausible reaction mechanism was proposed in Fig. S8. **NdSeW** activated the carbonyl groups of the aldehyde and benzil and then reacted with ammonia (generated *in situ* from ammonium acetate) to form imine intermediates **A** and **B**, respectively. The intermediate **A** condensed with the carbonyl group of **B** to give intermediate **C**, which finally undergoes dehydration and cyclization to afford the product **4a**.

Conclusions

In conclusion, we have successfully synthesized and characterized a novel neodymium-$\{SeO_3\}$-bridged selenotungstate (**NdSeW**). This compound features a distinctive architecture, in which $\{SeW_9\}$ and $\{SeW_8\}$ units are linked by an organometallic $\{Nd_2Se_2(mal)W_4\}$ cluster to form a triangular trimeric structure. Moreover, these trimers further self-assemble into an extended one-dimensional chain through alternating connections of neodymium and $\{SeO_3\}$ groups. Notably, **NdSeW** demonstrates high catalytic efficiency and versatility in the one-pot synthesis of 2,4,5-trisubstituted imidazoles *via* a three-component condensation of aldehydes, benzils, and ammonium acetate. The catalytic system proceeds under mild and environmentally friendly conditions, employing EtOH as a green solvent, with water as the sole by-product. This work not only enriches the structural diversity and synthetic methodology of Ln-POMs but also highlights their potential as sustainable catalysts for facilitating valuable organic transformations.

Conflicts of interest

There are no conflicts to declare.

Data availability

The data supporting this article have been included as part of the supplementary information (SI). Supplementary information is available. See DOI: https://doi.org/10.1039/d5dt02801a.

CCDC 2489933 (**NdSeW**) contains the supplementary crystallographic data for this paper.[40]

Acknowledgements

This work was financially supported by the National Natural Science Foundation of China (22301033) and the Jiangxi Provincial Natural Science Foundation (20212BAB213001).

References

1 H.-X. Bi, X.-Y. Yin, J.-Y. He, H. Song, S.-J. Lu, Y.-Y. Ma and Z.-G. Han, Conjugated organic component-functionalized hourglass-type phosphomolybdates for visible-light photocatalytic Cr(VI) reduction in wide pH range, *Rare Met.*, 2023, **42**, 3638–3650.
2 A. Bijelic, M. Aureliano and A. Rompel, Polyoxometalates as Potential Next-Generation Metallodrugs in the Combat Against Cancer, *Angew. Chem., Int. Ed.*, 2019, **58**, 2980–2999.
3 Y. Chen, Z.-X. Zhang, P.-W. Cai, Z.-W. Guo, Z.-W. Lu, C. Sun, X.-X. Li, J.-X. Chen, Z.-H. Wen and S.-T. Zheng, Polyoxotungstate Featuring Zinc-Ion-Triggered Structural Transformation as An Efficient Electrolyte Additive for Aqueous Zinc-Ion Batteries, *Angew. Chem., Int. Ed.*, 2025, **64**, e202420284.
4 J. Lei, Z. Yu, S. Ru, Z. Wang, S. Li, N. Luo, J. Huang, X. Peng, F. Jiang and Y. Wei, Decavanadate-Catalyzed Oxidative Cross-Dehydrogenative Coupling: an Efficient

and Sustainable Approach toward P(O)—S Bond Formation, *Angew. Chem., Int. Ed.*, 2025, **64**, e202507245.

5 H. Li, M. Yang, Z. Yuan, Y. Sun, P. Ma, J. Niu and J. Wang, Construction of one Ru_2W_{12}-cluster and six lacunary Keggin tungstoarsenate leading to the larger Ru-containing polyoxometalate photocatalyst, *Chin. Chem. Lett.*, 2022, **33**, 4664–4668.

6 S.-R. Li, W.-D. Liu, L.-S. Long, L.-S. Zheng and X.-J. Kong, Recent advances in polyoxometalate-based lanthanide–oxo clusters, *Polyoxometalates*, 2023, **2**, 9140022.

7 Y.-F. Liu, C.-W. Hu and G.-P. Yang, Recent advances in polyoxometalates acid-catalyzed organic reactions, *Chin. Chem. Lett.*, 2023, **34**, 108097.

8 Z.-Y. Liu, Y.-D. Lin, Y. Hao, H.-N. Chen, Z.-W. Guo, X.-X. Li and S.-T. Zheng, Recent advances in polyoxoniobate-catalyzed reactions, *Tungsten*, 2022, **4**, 81–98.

9 G. Yang, Y. Liu and Y. Wei, Application of polyoxometalates in biomass conversion, *Coord. Chem. Rev.*, 2024, **521**, 216172.

10 X. Huang, S. Liu, G. Liu, Y. Tao, C. Wang, Y. Zhang, Z. Li, H. Wang, Z. Zhou, G. Shen, Z. Xue and D. Sun, An unprecedented 2-fold interpenetrated lvt open framework built from Zn6 ring seamed trivacant polyoxotungstates used for photocatalytic synthesis of pyridine derivatives, *Appl. Catal., B*, 2023, **323**, 122134.

11 C. Lian and G.-Y. Yang, A tetrameric polyoxometalate with two orderly and dense double-layered $\{Ni_{12}W_{8/3}\}$ cluster centers, *Chem. Commun.*, 2025, **61**, 14402–14405.

12 G. Liu, Y. Chen, Y. Chen, Y. Shi, M. Zhang, G. Shen, P. Qi, J. Li, D. Ma, F. Yu and X. Huang, Indirect Electrocatalysis S—N/S—S Bond Construction by Robust Polyoxometalate Based Foams, *Adv. Mater.*, 2023, **35**, 2304716.

13 L. Liu, J. Jiang, X. Liu, G. Liu, D. Wang, L. Chen and J. Zhao, First series of mixed (PIII, SeIV)-heteroatom-oriented rare-earth-embedded polyoxotungstates containing distinct building blocks, *Inorg. Chem. Front.*, 2020, **7**, 4640–4651.

14 X. Zhang, H. Li, N. Xu, X. Liu and X.-L. Wang, Engineering geometric metamorphosis in $\{P_6M_2Mo_{16}O_{73}\}$-based high-nuclearity metal superclusters: from tetrahedral to square assemblies via topological transformations, *Inorg. Chem. Front.*, 2025, **12**, 3823–3832.

15 C. Boskovic, Rare Earth Polyoxometalates, *Acc. Chem. Res.*, 2017, **50**, 2205–2214.

16 Y.-C. Dai, S.-Y. Zhang, X.-X. Xiao, M.-J. Li, J.-C. Liu, L.-J. Chen and J.-W. Zhao, A double-tartrate-bridged decanuclearity europium-tungsten cluster embedded selenotungstate and its selective optical sensing of o-nitrophenol, *Polyoxometalates*, 2023, **2**, 9140041.

17 D. Zhou, B. Li, Q. Zhao, X. Tang, T. Lan, H. Su, G. Yang and W. Xuan, Solvent-modulated assembly of peptide and cerium functionalized gigantic $\{Mo_{120}Ce_6\}_2$ dimers for high-efficiency photocatalytic oxidation, *Inorg. Chem. Front.*, 2024, **11**, 2355–2364.

18 J. M. Cameron, J. Gao, L. Vilà-Nadal, D.-L. Long and L. Cronin, Formation, self-assembly and transformation of a transient selenotungstate building block into clusters, chains and macrocycles, *Chem. Commun.*, 2014, **50**, 2155–2157.

19 J. Jiang, L. Liu, G. Liu, D. Wang, Y. Zhang, L. Chen and J. Zhao, Organic–Inorganic Hybrid Cerium-Encapsulated Selenotungstate Including Three Building Blocks and Its Electrochemical Detection of Dopamine and Paracetamol, *Inorg. Chem.*, 2020, **59**, 15355–15364.

20 L. Liu, J. Jiang, L. Cui, J. Zhao, X. Cao and L. Chen, Double Trigonal Pyramidal $\{SeO_3\}$ Groups Bridged 2-Picolinic Acid Modified Cerium-Inlaid Polyoxometalate Including Mixed Selenotungstate Subunits for Electrochemically Sensing Ochratoxin A, *Inorg. Chem.*, 2022, **61**, 1949–1960.

21 J. Yan, D.-L. Long and L. Cronin, Development of a Building Block Strategy To Access Gigantic Nanoscale Heteropolyoxotungstates by Using SeO32− as a Template Linker, *Angew. Chem., Int. Ed.*, 2010, **49**, 4117–4120.

22 W.-C. Chen, H.-L. Li, X.-L. Wang, K.-Z. Shao, Z.-M. Su and E.-B. Wang, Assembly of Cerium(III)-Stabilized Polyoxotungstate Nanoclusters with SeO_3^{2-}/TeO_3^{2-} Templates: From Single Polyoxoanions to Inorganic Hollow Spheres in Dilute Solution, *Chem. – Eur. J.*, 2013, **19**, 11007–11015.

23 H.-L. Li, Y.-J. Liu, Y.-M. Li, L.-J. Chen, J.-W. Zhao and G.-Y. Yang, Unprecedented Selenium and Lanthanide Simultaneously Bridging Selenotungstate Aggregates Stabilized by Four Tetra-vacant Dawson-like $\{Se_2W_{14}\}$ Units, *Chem. – Asian J.*, 2018, **13**, 2897–2907.

24 H.-L. Li, S.-H. Zhao, N.-H. Wang, Y.-L. Ma, C. Lian and X. Cao, Se-Rich Multinuclear Er-Containing Dawson-type Poly(selenotungstate), *Inorg. Chem.*, 2024, **63**, 21645–21651.

25 W.-C. Chen, L.-K. Yan, C.-X. Wu, X.-L. Wang, K.-Z. Shao, Z.-M. Su and E.-B. Wang, Assembly of Keggin-/Dawson-type Polyoxotungstate Clusters with Different Metal Units and SeO_3^{2-} Heteroanion Templates, *Cryst. Growth Des.*, 2014, **14**, 5099–5110.

26 G. Liu, L. Liu, T. Gong, Y. Li, L. Chen and J. Zhao, Nicotinic-Acid-Ornamented Tetrameric Rare-Earth-Substituted Phospho(III)tungstates with the Coexistence of Mixed Keggin/Dawson Building Blocks and Its Honeycomb Nanofilm for Detecting Toxins, *Inorg. Chem.*, 2021, **60**, 14457–14466.

27 J.-C. Liu, J.-F. Wang, Q. Han, P. Shangguan, L.-L. Liu, L.-J. Chen, J.-W. Zhao, C. Streb and Y.-F. Song, Multicomponent Self-Assembly of a Giant Heterometallic Polyoxotungstate Supercluster with Antitumor Activity, *Angew. Chem., Int. Ed.*, 2021, **60**, 11153–11157.

28 Y. Gao, B. Mei, Y. Wu, Q. Zhao, Z. Bao, H. Qin, Y. Xu, H. Lv, X. Peng, Y. He, T. Luo, R. Yao, W. Zhang, H. Lei and R. Cao, A Cobalt(III) Corrole with a Tethered Imidazole for Boosted Electrocatalytic Oxygen Reduction Reaction, *Chin. J. Chem.*, 2023, **41**, 2866–2872.

29 K. Ravikumar and M. S. Dangate, Imidazole and thiazole derivatives: Synthesis, characterization, and nonlinear optical properties, *J. Mol. Struct.*, 2025, **1338**, 142287.

30 L. Zhang, X.-M. Peng, G. L. V. Damu, R.-X. Geng and C.-H. Zhou, Comprehensive Review in Current Developments of Imidazole-Based Medicinal Chemistry, *Med. Res. Rev.*, 2014, **34**, 340–437.

31 A. Alanthadka, S. D. Elango, P. Thangavel, N. Subbiah, S. Vellaisamy and U. M. Chockalingam, Construction of substituted imidazoles from aryl methyl ketones and benzylamines via N-heterocyclic carbene-catalysis, *Catal. Commun.*, 2019, **125**, 26–31.

32 J.-R. Chang, L. Cao, S. Jia, F. Fang, Z.-H. Fan, Q.-J. Pan, Y.-N. Ma and X. Chen, Synthesis of Imidazole Adducts of BH3, BF3, and B3H7 and Comparison of Their Nucleophilic Substitution Reaction Activity, *Chin. J. Chem.*, 2025, **43**, 925–930.

33 J. Jayram and V. Jeena, Copper-catalyzed aerobic benzylic sp3 C–H oxidation mediated synthesis of 2,4,5-trisubstituted imidazoles via a domino multi-component reaction, *Green Chem.*, 2017, **19**, 5841–5845.

34 D. Kumar, D. N. Kommi, N. Bollineni, A. R. Patel and A. K. Chakraborti, Catalytic procedures for multicomponent synthesis of imidazoles: selectivity control during the competitive formation of tri- and tetrasubstituted imidazoles, *Green Chem.*, 2012, **14**, 2038–2049.

35 X. Tian, L. Song, M. Rudolph, F. Rominger, T. Oeser and A. S. K. Hashmi, Sulfilimines as Versatile Nitrene Transfer Reagents: Facile Access to Diverse Aza-Heterocycles, *Angew. Chem., Int. Ed.*, 2019, **58**, 3589–3593.

36 C. T. F. Salfeena, R. Jalaja, R. Davis, E. Suresh and S. B. Somappa, Synthesis of 1,2,4-Trisubstituted-(1*H*)-imidazoles through $Cu(OTf)_2/I_2$-Catalyzed C–C Bond Cleavage of Chalcones and Benzylamines, *ACS Omega*, 2018, **3**, 8074–8082.

37 J. O. Strelnikova, N. V. Rostovskii, G. L. Starova, A. F. Khlebnikov and M. S. Novikov, Rh(II)-Catalyzed Transannulation of 1,2,4-Oxadiazole Derivatives with 1-Sulfonyl-1,2,3-triazoles: Regioselective Synthesis of 5-Sulfonamidoimidazoles, *J. Org. Chem.*, 2018, **83**, 11232–11244.

38 N. Hosseini Mohtasham and M. Gholizadeh, Magnetic horsetail plant ash (Fe_3O_4@HA): a novel, natural and highly efficient heterogeneous nanocatalyst for the green synthesis of 2,4,5-trisubstituted imidazoles, *Res. Chem. Intermed.*, 2021, **47**, 2507–2525.

39 M. Masteri-Farahani, A. Ezabadi, R. Mazarei, P. Ataeinia, S. Shahsavarifar and F. Mousavi, A new nanocomposite catalyst based on clay-supported heteropolyacid for the green synthesis of 2,4,5-trisubstituted imidazoles, *Appl. Organomet. Chem.*, 2020, **34**, e5727.

40 CCDC 2489933: Experimental Crystal Structure Determination, 2026, DOI: 10.5517/ccdc.csd.cc2pkzfp.